Robotica (2019) volume 37, pp. 1057–1072. © Cambridge University Press 2019
doi:10.1017/S0263574718001431

Kinematics-Based Simulation and Animation of Articulated Rovers Traversing Uneven Terrains

Mahmoud Tarokh* and Huy Dang Ho

Department of Computer Science, San Diego State University, San Diego, CA, 92182, USA.
E-mail: danghuyho@yahoo.com

(Accepted December 12, 2018. First published online: January 29, 2019)

SUMMARY
The paper develops a simulation and animation environment for high-mobility rovers based on kinematic modeling. Various kinematic chains starting from the rover body to the wheels are analyzed and aggregated to obtain the model of the rover body motion in terms of the wheel motions. This model is then used to determine the actuations of the joints, wheels speed, and steering motors to achieve a desired motion of the rover over uneven terrain while avoiding loss of balance and tip-over. The simulation environment consists of a number of modules, including terrain and trajectory generation, and kinematic models for rover actuation and navigation. The animation of the rover motion over various terrains is developed, which allows observing the rover from various viewpoints and interacting with the system through a graphical user interface. The performance of the overall system is demonstrated by modeling a high-mobility space exploration rover, and the responses of the rover on uneven terrains are provided, which show the usefulness of the proposed modeling, simulation, and animation scheme.

KEYWORDS: Rover motion simulation; Rover kinematic modeling; Rover animation.

1. Introduction

Articulated mobile robots are being increasing deployed in challenging environments and for difficult tasks. These robots find applications in space exploration, agriculture, search-and-rescue operations, and defense, just to mention a few. High-mobility rovers require complex mechanisms to enable them to move on uneven and rough terrains. More advanced robots, such as those in space applications, are also required to perform complex maneuvers. Due to the high cost of these robots, it is essential to develop motion models, simulation, and animation environments to test their performance and make possible changes to their mechanical design before actual manufacturing and deployment.

There have been a number of simulation studies on mobile robots and rovers from various viewpoints. Many rover simulation studies concentrate on the modeling of the wheel–terrain interaction using terra-mechanics.[1–3] The estimation of terrain parameters for traversability prediction and traction control is discussed in ref. [1]. The wheel–soil interaction mechanism is formulated in ref. [2] by evaluating traction forces for various slip conditions. A comprehensive review of various studies in wheel slippage and its estimation is provided in ref. [3]. In the work reported in ref. [4], the interaction between the wheel and terrain is simulated to obtain the contact parameters. The model of a rigid wheel and soft soil is used in ref. [5] to compute normal and shear stress distributions in the contact area. In a similar vein, an algorithm to compute the wheel–terrain contact area parameters as well as the contact velocity and force has been proposed.[6] The method in ref. [7] uses fractional Brown motion technique and statistical properties to generate a lunar surface and to develop a simulation environment with dynamics of the multi-body systems and interactions with the soft ground.

* Corresponding author. E-mail: mtarokh@sdsu.edu

A software tool to simulate rigid wheels as a planetary rover traversing across the natural terrain is reported in ref. [8]. All the above references provide models and simulations for the specific issue of wheel–terrain interaction from terra-mechanics viewpoint.

A numerical method for simulation of the trajectory response of a rover is presented in ref. [9]. Another study dealt with the numerical stability of the so-called inverse simulation.[10] An investigation of the thermal structure of a lunar rover under adverse conditions is performed in ref. [11] to predict the temperature profile at the lunar surface. Finally ref. [12] proposed a simulation study of the structures and mechanisms of three rovers to determine the most suitable one for applications in agriculture.

Articulated robots require sophisticated mobility mechanisms to enable them to traverse rough terrain. Several mobility systems are investigated in ref. [13] to determine their capabilities for a variety of natural terrains and for mars missions.[14] Various robot configurations and mechanisms suitable for agricultural applications are studied in ref. [15]. Actuator redundancy in multi-wheeled robot systems was shown to improve ground traction and to reduce power consumption.[16]

This paper deals with the modeling and simulation of articulated rovers from a kinematics viewpoint. It applies a full kinematic model for the simulation and animation of highly articulated rovers moving on uneven solid terrains. High-mobility rovers have complex suspension systems to enable them to modify and adjust their mechanism to cope with uneven terrains. As such their modeling and kinematic analysis presents challenging tasks. Until recently, research on mobile robot modeling was limited to simple robots moving on flat surfaces. Recently, research efforts on modeling have been extended to more complex robots and rovers. The earliest work on kinematic modeling of a high-mobility space robot appears to be ref. [17]. A fundamental research work on the modeling of general articulated rovers was subsequently published where various forms of kinematic models for articulated robots were introduced.[18] The balance control of rovers to avoid tip-over is reported in ref. [19], and systematic modeling of high-mobility rovers was developed in ref. [20].

In this paper we first provide an overview in Section 2, drawing material from our previous publication[20] on kinematic modeling, and then provide a compact formulation that is suitable for the simulation of high-mobility rovers. Subsequently in Section 3, we describe the structure of our simulation and animation and describe the various modules that were developed. The results are provided in Section 4 for a space rover where kinematic modeling is applied, the trajectories of various rover quantities are shown, and the motions of the rover over different terrains are displayed. Conclusions are given in Section 5.

2. Overview of General Rover Kinematic Analysis

Broadly speaking, robots can be categorized into manipulators and mobile robots. A manipulator consists of a chain of links and joints starting from a fixed base and terminating at an end-effector for manipulating objects. A mobile robot consists of a base and a suspension system that has links and joints terminating at wheels for rolling on the terrain. Rovers are a class of mobile robots that have complex suspension systems that enable them to move over rough terrains.

The standard method of kinematic modeling for manipulators is to assign frames on links and apply a transformation matrix that transforms the position and orientation of a frame F_{i-1} to those of the neighboring frame F_i. We denote the position and orientation of frame F_i, respectively, by $u_i = (x_i, y_i, z_i)$ and $\varphi_i = (\alpha_i, \beta_i, \gamma_i)$; $i = 1, 2, \ldots, n$, where α_i, β_i, and γ_i are roll, pitch, and yaw, respectively, and n is the number of frames between the manipulator base and the end-effector (hand). The transformation matrix from frame $(i-1)$ to frame (i) is described by four so-called "D–H" parameters $(\varepsilon_i, a_i, \Theta_i, d_i)$, where $(\varepsilon_i, \Theta_i)$ are angles and (a_i, d_i) are lengths, suitably defined.[21] Furthermore, (ε_i, a_i) are associated with the link between two frames and are fixed, whereas Θ_i, or d_i is variable. A joint can be revolute in which case $d_i = 0$, or prismatic where $\Theta_i = 0$.

Unlike serial manipulators that have one kinematic chain, rovers have several chains each starting at the same rover body location but ending at different wheels. In addition, in the case of rovers, motion takes place over the terrain. As a result, we must transform the translational and rotational velocities of frame $(i-1)$ in the jth chain denoted by $F_{i-1,j}$ to those of frame (i) in the same chain j denoted by F_{ij}. It is to be noted that in the case of motion, in addition to the four parameters $(\varepsilon_{ij}, a_{ij}, \Theta_{ij}, d_{ij})$, we must include the rate of change of these parameters, that is, $\dot{\Theta}_{ij}$ or $\dot{d}_{ij}$, noting that $\dot{\varepsilon}_{ij} = \dot{a}_{ij} = 0$ since ε_i and a_i are related to link lengths, which are constant. Consequently, for

https://doi.org/10.1017/S0263574718001431 Published online by Cambridge University Press

rovers we have five parameters, that is, $(\varepsilon_{ij}, a_{ij}, \Theta_{ij}, d_{ij}, \dot{\Theta}_{ij})$ or $(\varepsilon_{ij}, a_{ij}, \Theta_{ij}, d_{ij}, \dot{d}_{ij})$ describing the frame-to-frame velocity transformation.

Using the developments in ref. [20], it can be shown that the equation of motion from frame $F_{i-1,j}$ to frame F_{ij} is

$$\begin{pmatrix} \dot{u}_{ij} \\ \dot{\varphi}_{ij} \end{pmatrix} = \begin{pmatrix} R_{ij} & R_{ij}S_{ij} \\ 0 & R_{ij} \end{pmatrix} \begin{pmatrix} \dot{u}_{i-1,j} \\ \dot{\varphi}_{i-1,j} \end{pmatrix} + b\dot{\eta}_{ij};\ i = 1, 2, \ldots, n_j; j = 1, 2, \ldots, m \tag{1}$$

where R_{ij} and S_{ij} are, respectively, a rotation matrix and a skew symmetric matrix given in Eq. (2), and n_j is the number of frames between the rover body and wheel j. If joint i in chain j is prismatic, it affects the z component of the position vector $\dot{u}_{ij}$; thus $b = (0\ 0\ 1\ 0\ 0)^T$ and $\dot{\eta}_{ij} = \dot{d}_{ij}$. On the other hand, if the joint is revolute, it affects the yaw components of the orientation vector $\dot{\varphi}_{ij}$ and in this case $b = (0\ 0\ 0\ 0\ 1)^T$ and $\dot{\eta}_{ij} = \dot{\theta}_{ij}$.

$$R_{ij} = \begin{pmatrix} \cos\theta_{ij} & \cos\varepsilon_{ij}\sin\theta_{ij} & \sin\varepsilon_{ij}\sin\theta_{ij} \\ -\sin\theta_{ij} & \cos\epsilon_{ij}\cos\theta_{ij} & \sin\varepsilon_{ij}\cos\theta_{ij} \\ 0 & -\sin\varepsilon_{ij} & \cos\varepsilon_{ij} \end{pmatrix}; S_{ij} = \begin{pmatrix} 0 & \mathrm{d}_{ij}\cos\varepsilon_{ij} & \mathrm{d}_{ij}\sin\varepsilon_{ij} \\ -\mathrm{d}_{ij}\cos\varepsilon_{ij} & 0 & \mathrm{a}_{ij} \\ -\mathrm{d}_{ij}\sin\varepsilon_{ij} & -\mathrm{a}_{ij} & 0 \end{pmatrix} \tag{2}$$

Note that the 3×3 matrices R_{ij} and S_{ij} are functions of the parameters $(\varepsilon_{ij}, a_{ij}, \Theta_{ij}, d_{ij})$ and that S_{ij} is a skew symmetric matrix. Equation (1) can be put into a more compact form as

$$\dot{v}_{ij} = P_{ij}\dot{v}_{i-1,j} + b\ \dot{\eta}_{ij};\ i = 1, 2, \ldots, n_j; j = 1, 2, \ldots, m \tag{3}$$

where $\dot{v}_{ij} = \begin{pmatrix} \dot{u}_{ij} \\ \dot{\varphi}_{ij} \end{pmatrix}$ is a 3×1 vector of configuration velocity, which is the combination of position and orientation velocities, and P_{ij} is a 6×6 matrix defined in Eq. (1). Cascading the transformations in Eq. (3), we obtain the relationship between wheel velocities and rover body velocities as

$$\dot{v}_{wj} = P_j\ \dot{v}_b + Q_j\dot{\eta}_j;\ j = 1, 2, \ldots, m \tag{4}$$

where the wheel is at the end of the chain $(i = n_j)$ so that $\dot{v}_{wj} \equiv \dot{v}_{n,j}$ is the configuration velocity vector of wheel j, and $\dot{v}_b = \dot{v}_{o1} = \dot{v}_{o2} = \cdots = \dot{v}_{oj}$ is the rover reference body configuration velocity, which is common for all chains, and $\dot{\eta}_j = \left(\dot{\eta}_{1j}^T \ldots \dot{\eta}_{n_j}^T\right)^T$ is the $n_j \times 1$ vector of chain joint velocity. The matrices in Eq. (4) are a 6×6 matrix $P_j = P_{n_j} \ldots P_{2j}P_{1j}$ and a $6 \times n_j$ matrix $Q_j = \left((P_{nj} \ldots P_{2j}b)\ (P_{nj} \ldots P_{3j}b) \cdots \left(P_{nj}b\right)\ (b)\right)$. We refer to Eq. (4) as *contact kinematics* since it makes it possible to compute the wheel velocities at contact with the terrain for a given desired motion of the rover body having velocity $\dot{v}_b$ and chain joint velocity vector $\dot{\eta}_j$ associated with the jth wheel. We can also determine the motion of the body by measuring the wheel velocities. This is done by pre-multiplying Eq. (4) by the inverse of P_j to obtain

$$\dot{v}_b = G_j\dot{v}_{wj} + H_j\ \dot{\eta}_j;\ j = 1, 2, \ldots, m \tag{5}$$

where $G_j = \left(P_j\right)^{-1}$ and $H_j = -\left(P_j\right)^{-1}Q_j$. Equation (5) describes the contributions of individual wheels to the rover body motion. The net body motion is the composite effect of the motions of all wheels, which can be obtained by aggregation the m equations in (5) as

$$E\dot{v}_b = G\dot{v}_w + H\dot{\eta} \tag{6}$$

where $E = \begin{pmatrix} I_6 \\ \vdots \\ I_6 \end{pmatrix}$ is a $6m \times 6$ matrix; I_6 is a 6×6 identity matrix; $G = blockdiag\left\{G_j\right\}$ is a $6m \times 6m$ aggregate matrix; $H = blockdiag\left\{H_j\right\}$ is a $6m \times \sum_{j=1}^{m} n_j$ aggregate matrix; $\dot{v}_w = (\dot{v}_{w1} \cdots \dot{v}_{wm})^T$ is a $6m \times 1$ vector of the aggregate wheel velocities; and $\dot{\eta} = (\dot{\eta}_1 \cdots \dot{\eta}_m)^T$ is a $(\sum_{j=1}^{m} n_j) \times 1$ velocity vector of all joint variables in the various frames and chains. It is noted that some joints are actuated and others are passive/compliant. The actuated joints can be controlled, while the passive joints vary to comply with the terrain, that is, to make the wheels touch uneven terrain. We referred to Eq. (6) as navigation kinematics.

https://doi.org/10.1017/S0263574718001431 Published online by Cambridge University Press

There is little practical use for the navigation kinematics (Eq. 6) on its own due to wheel slippage, which might result in odometry errors. However, Eq. (6) is very useful for deriving the *actuation kinematics*, which is determining the commands to the actuators so that the rover body moves along a desired trajectory while achieving balanced rover configurations. The latter is required to avoid tip-over when the rover traverses on a rough terrain. Actuators consist of wheel and steering motors as well as joint motors (linear or rotational) that exist in a high-mobility rover.

We can partition the quantities in Eq. (6) into two sets of known and unknown. The known quantities are the measured (sensed) and specified quantities. Rovers are generally equipped with sensors such as accelerometers for measuring body pitch and roll angles, and joint values. The specified quantities are forward velocity of the rover body $\dot{x}_b$ and its yaw rate $\dot{\gamma}_b$. The specified quantities can also include some wheel slips such as tilt rate $\dot{\alpha}_j$ and sway rate β_j; $j = 1, 2, \ldots, m$ that are set to 0 because of the mechanical construction that does not allow these motions. The unknown quantities consist of the actuation quantities that need to be determined for the desired body motion, as well as quantities that are non-measureable. The actuation quantities are the wheel roll rates $\dot{\vartheta}_j$, as well as articulated body actuators, such as steering, that constitute some components of $\dot{\eta}$ in Eq. (6). In the following formulation, the known quantities are identified by a bar superscript and unknown are denoted by a tilde superscript. With these notations, the partitioning of Eq. (6) into known and unknown quantities become

$$\left(\tilde{E}\ \bar{E}\right)\begin{pmatrix}\tilde{\dot{v}}_b\\ \bar{\dot{v}}_b\end{pmatrix} = \left(\tilde{G}\ \bar{G}\right)\begin{pmatrix}\tilde{\dot{v}}_w\\ \bar{\dot{v}}_w\end{pmatrix} + \left(\tilde{H}\ \bar{H}\right)\begin{pmatrix}\tilde{\dot{\eta}}\\ \bar{\dot{\eta}}\end{pmatrix} \tag{7}$$

where $\tilde{\dot{v}}_b$ and $\bar{\dot{v}}_b$ are, respectively, the unknown and known vectors of the body configuration velocities; $\tilde{\dot{v}}_w$ and $\bar{\dot{v}}_w$ are the corresponding wheel quantities; and $\tilde{\dot{\eta}}$ and $\bar{\dot{\eta}}$ are the actuated and passive joint vectors. The actuation quantities are the adjustable joint angles, such as steering and wheel rolling that allow control over the rover, and the passive joints enable compliance of the rover with the terrain.

Equation (7) can be rearranged by separating the known and unknown quantities:

$$\left(\tilde{E}\ -\tilde{G}\ -\tilde{H}\ \right)\begin{pmatrix}\tilde{\dot{v}}_b\\ \tilde{\dot{v}}_w\\ \tilde{\dot{\eta}}\end{pmatrix} = \left(-\bar{E}\ \bar{G}\ \bar{H}\right)\begin{pmatrix}\bar{\dot{v}}_b\\ \bar{\dot{v}}_w\\ \bar{\dot{\eta}}\end{pmatrix} \tag{8a}$$

$$\mathcal{A}\mathcal{X} = \mathcal{B}\mathcal{Y} \tag{8b}$$

where $\mathcal{X}$ and $\mathcal{Y}$ are, respectively, vectors of unknown and known quantities, and $\mathcal{A}$ and $\mathcal{B}$ are matrices defined in Eq. (8a). In a high-mobility rover, there are more actuated and compliant (unknown) quantities than the measured and specified (known) quantities. This allows specifying optimization of a performance criterion $\mathcal{F}$ such as balancing the rover when it traverses rough terrain to avoid tip-over, and also to keep the actuated joint angles $\tilde{\eta}$ close to their nominal (mid-range) values $\tilde{\eta}_n$ to avoid actuator saturation. A rover moving on a flat surface has zero body roll α_b and pitch β_b and operates close to its nominal joint values. Balancing criterion is achieved by keeping the body roll α_b and pitch β_b and deviation of the actuated joint as close to 0 as possible. Thus, a suitable performance criterion is

$$\mathcal{F} = a_1\|\tilde{\eta} - \tilde{\eta}_n\| + a_2\,\alpha_b^2 + a_3\beta_b^2 \tag{9}$$

where a_1, a_2, and a_3 are some weighting constants. By minimizing Eq. (9), the first term keeps the angles as close as possible to their nominal values, and the second and third terms attempt to keep the rover flat. A solution to the linear system of Eq. (8b) subject to minimization criterion Eq. (9) has been obtained in ref. [22].

$$\mathcal{X} = \mathcal{A}^{\star}\mathcal{B}\,\mathcal{Y} + k\left(E - \mathcal{A}^{\star}\mathcal{A}\right)\begin{pmatrix}\frac{\partial\mathcal{F}}{\partial\tilde{\eta}}\\ 0\end{pmatrix} \tag{10}$$

where $\mathcal{A}^{\star}$ is the pseudo-inverse of $\mathcal{A}$ and the 0 vector accounts for the fact that the dimension of the vector $\frac{\partial\mathcal{F}}{\partial\tilde{\eta}}$ is less than the number of rows of $(E - \mathcal{A}^{\star}\mathcal{A})$. The gradient $\frac{\partial\mathcal{F}}{\partial\tilde{\eta}}$ is computed numerically at each operating point.

https://doi.org/10.1017/S0263574718001431 Published online by Cambridge University Press

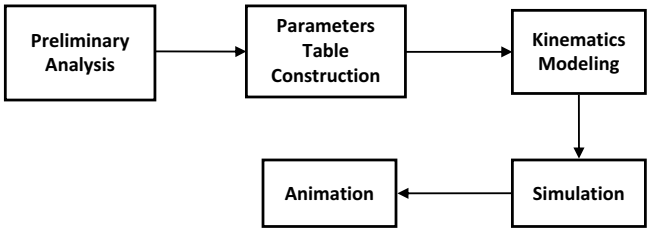

Fig. 1. Overall structure of the simulation and animation scheme.

3. Rover Motion Simulation and Animation

We developed a simulation environment for rovers based on the developments in Section 2 using Matlab Symbolic Math Toolbox. This toolbox integrates symbolic mathematics and variable precision computation. With this toolbox, numeric and symbolic computation can be combined into a single environment without sacrificing speed or accuracy. The goal is to make the developed simulations applicable to rovers of various mechanisms and suspension systems.

The simulation program consists of five main tasks as shown in Fig. 1. The preliminary analysis block represents the task needed to examine the structure of the rover in terms of linkages and suspension system and assign appropriate frames. Based on these frame assignments, the parameter table of the robot is set up. The kinematic modeling module uses this table to derive contact, navigation, and actuation kinematics discussed in Section 2. The simulation module utilizes the information provided by the kinematic module to compute the actuation signals such as joint velocities, wheel velocities, and steering rates based on the desired rover navigation quantities such as desired rover path trajectory. Finally, the animation module visualizes the motion of the rover on the terrain in 3D. In the subsections below, we discuss each of these modules in more detail.

3.1. Preliminary analysis

The first task is to examine the mechanical structure of the rover such as the number of wheels, that is, the manner in which the links and joints are arranged in kinematic chains connecting the rover body to the wheels. This information is utilized to set up the parameter table in a systematic method as demonstrated in the case study of Section 4.

3.2. Parameter table

The parameter table contains information about joints and links, that is, $(\varepsilon_{ij}, a_{ij}, \Theta_{ij}, \dot{\eta}_{ij})$ of each frame i in the kinematic chain j as mentioned in Section 2. For the analytical purpose, equations of motion mostly involve symbolic representation. Therefore, instead of using a regular text file to represent rover's characteristics and its parameter table, a Matlab's M-file is employed to declare the symbolic variables and symbolic expressions. Once the file is created, it can be used to obtain the following information.

- Rover's constant quantities such as height, width, length of rover, leg length, wheel radius, etc.
- A set of joint values for each linkage connecting the main body to a wheel.
- Steering angles, rolling angles, and contact angles as well as their rates (derivatives).
- Unknown and known quantities for contact, navigation, and actuation kinematics.

The rover parameters are arranged in such a way that the original parameter table is divided into sub-tables that correspond to kinematic chains from the main body to all wheels The structure of the file makes it convenient to adapt and generate profiles for different rovers.

3.3. Kinematic modeling

Various components of the "kinematic modeling" module in Fig. 1 are shown in some detail in Fig. 2. The translational velocities $(\dot{x}_b, \dot{y}_b, \dot{z}_b)$ and rotational velocities $(\dot{\alpha}_b, \dot{\beta}_b, \dot{\gamma}_b)$ of the rover reference body are defined in symbolic form. Subsequently, the kinematic module derives transformation matrices for each frame in the kinematic chains using Eqs (2) and (3). The contact kinematics is set up by aggregating the motions of different frames leading to a wheel as described by Eq. (4). For

https://doi.org/10.1017/S0263574718001431 Published online by Cambridge University Press

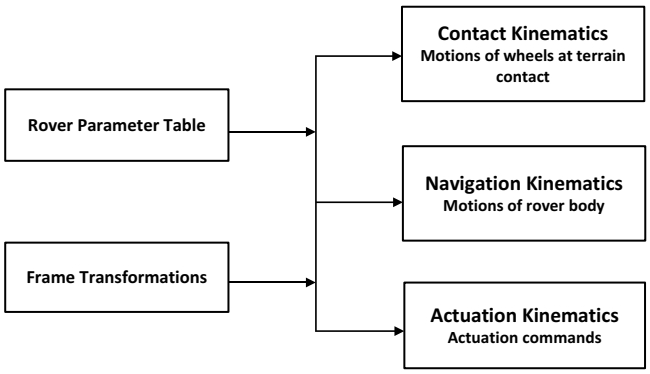

Fig. 2. Various components of the kinematic modeling.

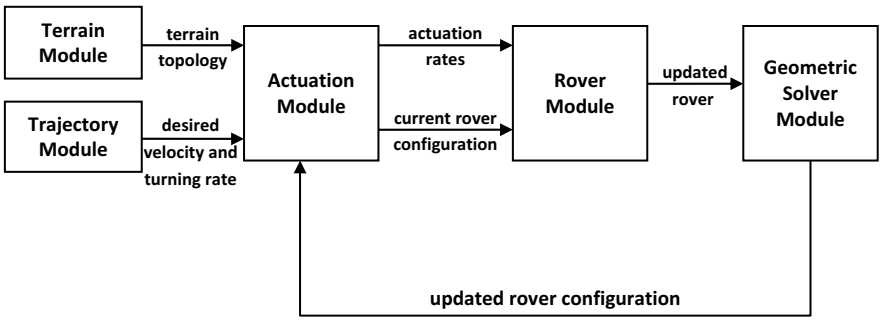

Fig. 3. Components of the simulation.

navigation kinematics, a reverse process is performed in which the combined effects of motions at wheel contacts determine the rover body motion using Eqs (5) and (6).

For a more useful form of the kinematics, namely, actuation kinematics, a further step is taken to partition and rearrange Eq. (6) into known and unknown quantities as in Eq. (7). The program examines each symbolic expression to determine if it contains any unknown by checking the list of known/unknown in the parameter table. All computed matrices, for example, E, G, and H in Eq. (7), are saved in a Matlab M-file with predefined naming convention. A major challenge in this kinematic synthesis is to find the right set of known and unknown quantities in order to identify the contribution of each unknown quantity to the overall body motion. A Matlab program is designed and written in such a way that the whole process is accomplished automatically, including the task of finding and partitioning the known/unknown quantities. To perform numeric computation, we only need to assign numeric values to symbolic variables and call proper functions. All expressions and matrices are evaluated with the help of Symbolic Math Toolbox.

3.4. Simulation

The Matlab configuration file resulting from the kinematic modeling module in Figs. 1 and 2 keeps all the required data to perform the simulation and controls the whole process. As shown in Fig. 3, there are five main modules involved in the simulation process, namely, generating the desired trajectories for the rover motion, generating various types of terrains, performing the actuations, updating the rover body configuration, and solving rover geometry to fit into the terrain. Each of these modules is briefly explained below.

3.4.1. Terrain and trajectory modules. This module produces a desired terrain for the rover motion. The parameters specifying the terrain topology consist of its width W along y-axis and length L along x-axis, and its elevation Z as a function of X and Y values of the terrain. A set of predefined terrains, from simple to complex topology, has been created as shown in Fig. 4, all of which are assumed to be solid so that the penetration of wheels into the ground does not take place. The performance of the rover when traversing these terrains is evaluated.

https://doi.org/10.1017/S0263574718001431 Published online by Cambridge University Press

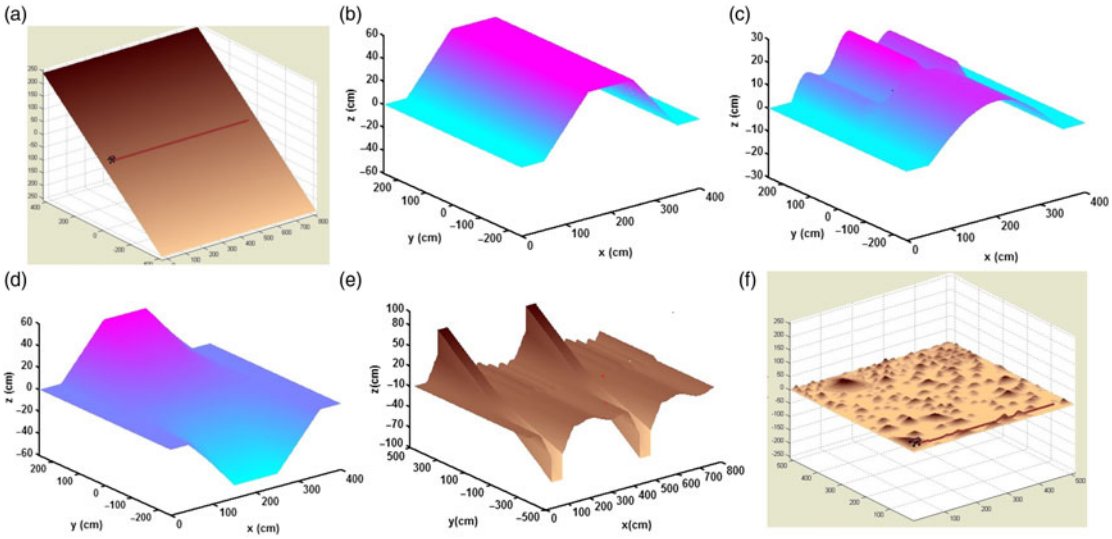

Fig. 4. Various terrain topologies used to test the performance of the rover; the unit on the axes is cm.

Figure 4a shows a terrain with a downward slope. The terrain in Fig. 4b has a ramp up followed by constant elevation and then a ramp down. The terrain in Fig. 4c consists of a half-period sinusoidal bump on the right and another sinusoid with higher frequency on the left. A ramp on the left and a ditch (ramp down) on the right constitute the terrain of Fig. 4d. A more complex version of Fig. 4d with several ramps and ditches is shown in Fig. 4e. Finally, a complex terrain is created in Fig. 4f by adding a random number of bumps of various shapes and heights placed at random locations on the terrain. Each of the above terrains is created using an appropriate mathematical function. For example, the terrain in Fig. 4b is described by

$$Z(X, Y) = \begin{cases} h \sin\left(\frac{2\pi}{p}(X - w)\right), & 0 \leq X \leq w \\ 0, & w < X \leq W \end{cases} \tag{11}$$

where h, w, and p are, respectively, the height, width, and period of the sinusoidal wave, and W is the width of the terrain. This type of terrain can be used to test the ability of the rover to balance itself when one side moves on the wavy region and the other side travels on a flat surface.

A trajectory is a description of the path parameterized by time that the rover reference frame, located at the center of the top platform, is required to follow on the terrain. It is represented by functions $X(t)$ and $Y(t)$. The rover yaw or heading is obtained from $\gamma = \frac{dY}{dX} = \frac{\dot{Y}}{\dot{X}}$. Examples of the trajectory are straight line where $X(t) = X_0 + at$, $Y(t) = Y_0 + bt$, with (X_0, Y_0) being the initial coordinates and (a, b) being some constants. A circular trajectory can be obtained by setting $X(t) = X_0 + r\ \cos(t)$ and $Y(t) = X_0 + r\ \sin(t)$ where (X_0, Y_0) is the center of the circle and r is its radius. More complex trajectories, such as serpentine, are similarly defined.

3.4.2. Actuation and rover modules. As discussed in Section 2, the actuation kinematics in Fig. 3 is concerned with determining the actuation signals as a function of the desired rover navigation quantities, such as rover position in the world coordinates $(X_b(t), Y_b(t))$, heading $\gamma_b(t)$, and measured (known) quantities such as rover body roll $\alpha_b(t)$ and pitch $\beta_b(t)$. The rover quantities and their rates in the world coordinates are transformed to the local/rover coordinates. The actuation signals are the wheel velocities, steering angles, etc., which are sent to the motors to achieve the desired rover position and orientation.

The actuation module at each time step $t = k\Delta t$, $k = 1, 2, \ldots$ receives two sets of inputs, which are either measured or computed from available data. The first set consists of the desired rover velocity $\dot{x}_b$ and rover heading rate $\dot{\gamma}_b$. The second set of inputs to the actuation module is the sensed data, which are the current states of the rover, for example, roll, pitch, and yaw angles, joint values, steering angles, etc.

https://doi.org/10.1017/S0263574718001431 Published online by Cambridge University Press

The output of this module at time $t = (k + 1)\Delta t$ is a set of estimated rates, namely, roll and pitch rates, joint rates, wheel rolling rate, steering rates, and slip rates, which are fed to the actuation module as the input, as mentioned in Section 2. In order to achieve these rates, Eq. (8a) is solved. The matrices $\mathcal{A}$ and $\mathcal{B}$ and the vector $\mathcal{Y}$ are set up and loaded into memory in the symbolic format. The actual numerical values are evaluated at each time step based on the current values of the measured or computed quantities. It must be noted that the solution $\mathcal{X}$ obtained using Eq. (10) ensures balancing of the rover to avoid tip-over.

The rover module in Fig. 3 is designed to work with current rover configuration. There are two sets of inputs to this module. The first is the actuation commands, which are the output of the actuation module. The second is the current state vector of the rover, which consists of the body position rate $\dot{u}_b = (\dot{x}_b, \dot{y}_b, \dot{z}_b)$, the orientation rate $\dot{\varphi}_b = (\dot{\alpha}_b, \dot{\beta}_b, \dot{\gamma}_b)$, and the actuated joint angle vector rate $\dot{\tilde{\eta}}$, which includes steering and suspension joint angle rates. The integration of these rates takes place in this module. In addition, the acquired joint angles, after the integration of their rates, are checked to ensure they are within their limits. In case the limits are exceeded, they are set to their limit. The output of the rover module is the updated rover state, which includes body position and orientation (rover configuration) and various joint angles.

3.4.3. Rover–terrain conforming module. The task involved in this module is to ensure that the rover is in contact with the terrain. In an actual rover moving on a rough terrain, the rover wheels make contact with the terrain naturally by changing its free variables. These variables include compliant (non-actuated) joints that exist in the rover suspension system as well as roll α_b, pitch β_b, and elevation z_b that are not fixed or specified for the rover trajectory. However, in simulations we must adjust the rover free variables to ensure that wheels contact with the terrain. Therefore, after each time increment, when the actuation takes place and rover moves incrementally to its next location, the free variable are adjusted to keep the wheels in contact with the terrain as much as possible. This is done by minimizing the distance between the wheels and the terrain below the wheels, as formulated below.

First, we must transform the position $u_b = (x_b, y_b, z_b)$ and orientation $\varphi_b = (\alpha_b, \beta_b, \gamma_b)$ of the rover body from its local coordinate $v_b = \begin{pmatrix} u_b \\ \varphi_b \end{pmatrix}$ to the world (terrain) coordinates $V_b = \begin{pmatrix} U_b \\ \Phi_b \end{pmatrix}$. Next, we perform a sequence of homogeneous transformations for various frames starting at the wheel j frame and ending at the rover body frame to relate the wheel j configuration V_{wj} to the rover body configuration V_b to obtain

$$V_{w_j}\left(U_b, \Phi_b, \eta_j\right) = T_{w_j b}\left(\eta_j\right)\ V_b(U_b, \Phi_b); j = 1, 2, \ldots, m \tag{12}$$

where $T_{w_j b}(\eta_j)$ is a 4×4 transformation matrix that is a function of joint variables η_j between body reference frame and the jth wheel. The body configuration vector V_b consists of position U_b and orientation Φ_b in the world coordinates. As a result, the configuration vector at the wheel contact point $V_{w_j}\left(U_b, \Phi_b, \eta_j\right)$ is a function of U_b, Φ_b, and joint vector η_j. The third component of the configuration vector $V_{w_j}\left(U_b, \Phi_b, \eta_j\right)$, that is, $Z_{w_j}\left(U_b, \Phi_b, \eta_j\right)$, is the elevation of the wheel and can be used to find the vertical distance denoted by D_j between the wheel j and the terrain under the wheel as

$$D_j = Z_{w_j}\left(U_b, \Phi_b, \eta_j\right) - Z\left(X_{w_j}, Y_{w_j}\right); j = 1, 2, \ldots, m \tag{13}$$

where $Z(X_{w_j}, Y_{w_j})$ is terrain elevation at point (X_{w_j}, Y_{w_j}) below the wheel j. We must minimize the distance D_j for all wheels, that is, $D = \sum_{j=1}^{m} D_j^2$, to maintain wheel contact with the terrain. The free variables in Eq. (13) are rover body elevation Z_b, which is the third component of the position vector U_b as well as roll α_b and pitch β_b, which are first and second components of the orientation vector Φ_b; and the passive/compliant joint angle vector $\overline{\eta}_j$, which are the free components of η_j. The other variables in Eq. (13), that is, X_b, Y_b, and γ_b, are specified by the desired trajectory, as explained in Section 3.4.1. The minimization is performed using the Matlab function "fminbnd." This search method uses Golden Section search and parabolic interpolation. We iteratively apply the search function to each free variable until we converge on a solution. The result is a rover configuration that conforms to the terrain. It should be noted that depending on the terrain topology and suspension system of the rover, it is possible that not all wheels can be in contact with the terrain at every time increment.

https://doi.org/10.1017/S0263574718001431 Published online by Cambridge University Press

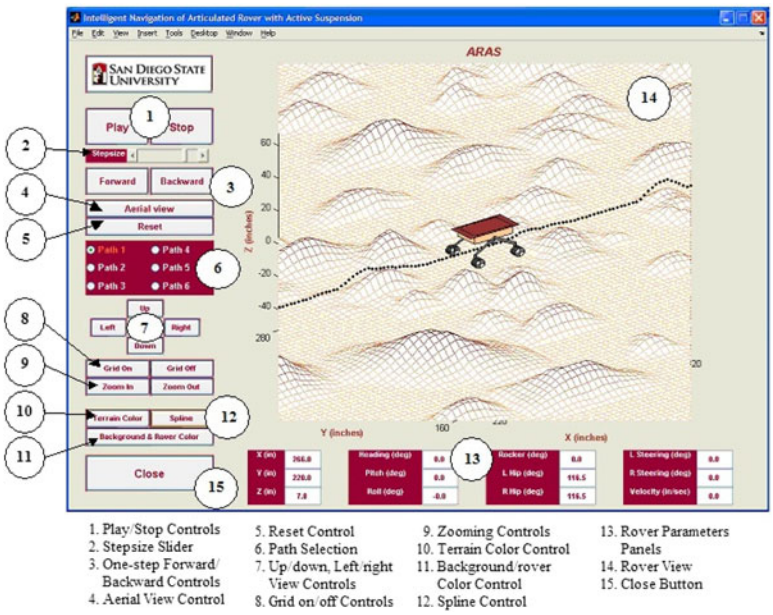

Fig. 5. Animation environment and its various facilities and options.

For the simulation purpose we have dealt only with a method for conforming the rover with solid terrains. The terra-mechanics and related issues, such as soil type and sinkage of wheels into the soil, are not included in the kinematic model. However, the proposed modeling and simulation environment allows including these aspects.

3.4.4. Animation. The developments of the previous sections are used to create the graphical interface and animation in order to better understand the rover motion and the ability to interact with the rover model through a 3D environment. This involves drawing the terrain, the trajectory, and a skeleton of the rover showing various joints, linkages, and body, as shown in Fig. 5. It consists of the rover moving on the terrain, displaying various quantities of interest, such as rover joint angles, pitch, and roll. In the animation, various views of the rovers, for example, side and front views, can be seen with zoon-in, zoom-out, and other options as indicated in Fig. 5. The names and functions of various buttons, numbered 1 through 15, in the animation environment are provided below the figure. The animation shows the movements of the rover over an uneven terrain, and while the rover moves, various information such as x, y, z locations of the rover, its pitch, roll, yaw, steering, and hip angles are displayed continually.

4. Case Study: NASA's Sample Return Rover

The articulated rover with active suspension considered here is similar to the NASA Sample Return Rover (SRR) and is shown in Fig. 6, where the linkages in the left figure are contracted to raise the body in order to avoid collision with rocks underneath the body. This rover can also raise one side with respect to the other side to level its body when one side is on a slope and the other side is on a flat terrain.

A schematic diagram of one side of SRR to be analyzed is depicted in Fig. 7. The rover has four wheels with independently actuated steering and speed. The rotation angles of wheels are subscripted with a clockwise direction so that (ϑ_1, ϑ_4) are for the left side, as shown in Fig. 7, and (ϑ_2, ϑ_3) are for the right side, not shown. At either side of the rover, two legs are connected via an adjustable hip joint, as seen Fig. 6. The hip angle values on the left and right sides of the rover are denoted by $2\sigma_1$ and $2\sigma_2$, respectively. These joints are actuated (adjustable) to enable the rover to raise and lower as shown in Fig. 6. Through these hip joints, the rover can raise its body to avoid hitting rocks, and can also raise one side with respect to the other to balance it when one side is on a lower terrain relative to the other side. The two hips are connected to the body via a differential that has an angle ρ on the left side and $-\rho$ on the right side. On a flat surface, ρ is 0 but becomes non-zero when one

https://doi.org/10.1017/S0263574718001431 Published online by Cambridge University Press

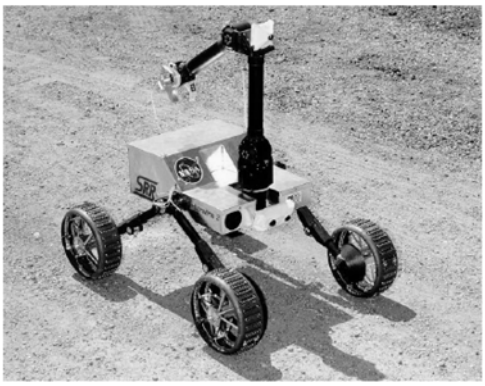

Fig. 6. NASA-JPL sample return rover.

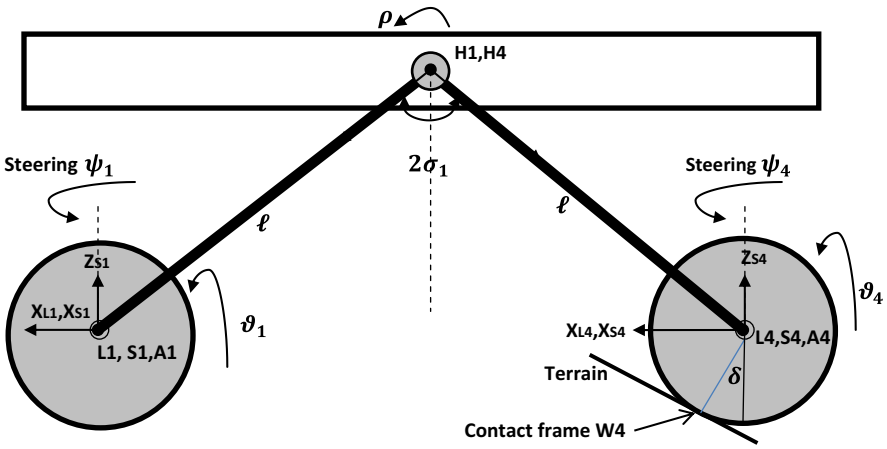

Fig. 7. Schematics of one side of the SRR with assignments of frames H, L, S, A, W, and variables ψ, ρ, δ.

side moves up or down with respect to the other. The differential joint ρ is passive (unactuated) and provides for the compliance with the terrain. The wheels are steerable with steering angles denoted by ψ_i, $i = 1, 2, 3, 4$.

4.1. Preliminary analysis and parameter table

We must now assign frames and set up the parameter table. Considering Fig. 6 we assign the frames as shown in Fig. 7. The center of gravity of the rover is chosen for the body reference frame $\{B\}$, which is the middle of the rover; the x-axis of the body is along the forward motion of rover; its y-axis is across the rover body; and z-axis points up to represent up and down motion. Differential frame $\{D\}$ is located at the middle of differential mechanism. The horizontal and vertical distance offsets from $\{B\}$ to $\{D\}$ are denoted by a_1 and d_1, respectively, which for our frame is $a_1 = d_1 = 0$. Furthermore, the half width of the rover is denoted by $d_2 = 20$ cm and each leg length is $\ell = 30$. The hip frames $\{H_1, H_4\}$ are located at the end of differential on the left side, and $\{H_2, H_4\}$ are at the right side of the differential. In addition, the origins of $\{H_1, H_4\}$ on the left side are coincident, and the same is true for the origins of $\{H_2, H_4\}$ on the right side. The leg frame L_j, steering frame S_j, and axel frame A_j share the same origin at the wheel center, as seen in Fig. 7. Finally, wheel–terrain contact frame is C_i and its x-axis is along the forward motion of the wheel. It is noted that the contact angle of the wheel with terrain δ_i is the angle between x-axis of the steering and axle frame, and r is the wheel radius.

The parameter table of the rover using the above frames is shown in Table I in a condensed form. In this table, various parameters are provided for each frame with $b_j = \begin{cases} 1 \text{ for } j = 1, 4 \\ -1 \text{ for } j = 2, 3 \end{cases}$ and $c_i = \begin{cases} 1 \text{ for } j = 2, 4 \\ -1 \text{ for } j = 1, 3 \end{cases}$. These constants are defined to make the parameter table compact, reducing the

https://doi.org/10.1017/S0263574718001431 Published online by Cambridge University Press

Table I. Parameter table for the SRR.

$\boldsymbol{F_{ij}}$	$\boldsymbol{\varepsilon_{ij}}$	$\boldsymbol{a_{ij}}$	$\boldsymbol{\Theta_{ij}}$	$\boldsymbol{d_{ij}}$	$\boldsymbol{\dot{\Theta}_{ij}}$
F_{Dj}	0	a_1	0	d_1	0
F_{Hj}	$-b_j 90$	0	$b_j 90 + \mathrm{c}_j\sigma_j + b_j\rho$	d_2	$\mathrm{c}_j\dot{\sigma}_j + b_j\dot{\rho}$
F_{Lj}	0	ℓ	$-b_j 90 - \mathrm{c}_j\sigma_j$	0	$-\mathrm{c}_j\dot{\sigma}_j$
F_{Sj}	$b_j 90$	0	ψ_j	0	$\dot{\psi}_j$
F_{Aj}	$-b_j 90$	ℓ	δ_j	0	$\dot{\delta}_j$
F_{Wj}	$b_j 90$	0	0	$-r$	0

number of rows for each frame from four to one. It is noted that there are two hip angles σ_1 and σ_2, but for notational convenience, four values are shown in Table I so that $\sigma_3 = \sigma_2$ and $\sigma_4 = \sigma_1$. In Table I, instead of denoting the six frames that exist between rover body and a wheel by $i = 1, 2, \ldots, 6$, they are shown as $i = D, H, L, S, A, W$, representing, respectively, differential, hip, leg, steering, axel, and wheel frames. It is noted that only $\dot{\Theta}_{ij}$ is non-zero due to the existence of revolute joints, and $\dot{\mathrm{d}}_{ij} = 0$ since there are no prismatic joints in this rover and therefore $\dot{\mathrm{d}}_{ij}$ is not included in Table I.

4.2. Kinematic modeling of SRR

The parameter table allows setting up the kinematic equations of the rover. Here we give, as an example, the results of motion transformation from a hip to a wheel using Eqs (1) and (2) and the third row of Table I.

$$\begin{pmatrix} \dot{u}_{Lj} \\ \dot{\varphi}_{Lj} \end{pmatrix} = \begin{pmatrix} k_j \sin\sigma_j & -b_j \cos\sigma_j & 0 & 0 & 0 & -b_j\ell\cos\sigma_j \\ b_j \cos\sigma_j & k_j \sin\sigma_j & 0 & 0 & 0 & k_j\ell\sin\sigma_j \\ 0 & 0 & 1 & 0 & -\ell_4 & 0 \\ 0 & 0 & 0 & k_j \sin\sigma_j & -b_i\cos\sigma_j & 0 \\ 0 & 0 & 0 & b_j\cos\sigma_j & k_j\sin\sigma_j & 0 \\ 0 & 0 & 0 & 0 & 0 & 1 \end{pmatrix} \begin{pmatrix} \dot{u}_{Hj} \\ \dot{\varphi}_{Hj} \end{pmatrix} + \begin{pmatrix} 0 \\ 0 \\ 0 \\ 0 \\ 0 \\ 1 \end{pmatrix} (-c_j)\dot{\sigma}_j; \quad j = 1, 2, 3, 4 \tag{14}$$

where $k_j = \begin{cases} 1 \text{ for } j = 1, 2 \\ -1 \text{ for } j = 3, 4 \end{cases}$. The other motion transformations from the rover body frame to the wheel–terrain contact can be similarly obtained. The aggregate motion transformation is then formed using Eqs (4)–(6) to obtain the navigation kinematics (6). Finally, the actuation kinematics incorporating optimization is derived.

4.3. Actuation

Let us first identify the known and unknown vectors in Eq. (8a) for the SRR. The rover forward body velocity $\dot{x}_b$ and rover direction (yaw rate) $\dot{\gamma}_b$ are specified by the desired trajectory and constitute a 2×1 vector of known quantity $\bar{\dot{\nu}}_b = (\dot{x}_b \;\; \dot{\gamma}_b)^T$. The remaining body configuration quantities form a 4×1 unknown body vector $\tilde{\dot{\nu}}_b = (\dot{y}_b \;\; \dot{z}_b \;\; \dot{\alpha}_b \;\; \dot{\beta}_b)^T$. The translational velocities of the wheels are $\dot{x}_{wj}, \dot{y}_{wj}, \dot{z}_{wj}$, where $\dot{x}_{wj} = r\dot{\vartheta}_{wj}$ in which $\dot{\vartheta}_{wj}$ is the wheel rolling velocity and r is the wheel radius. The wheel velocities $\dot{\vartheta}_{wj}, j = 1, 2, 3, 4$ are unknown actuated quantities and must be determined. The side slip $\dot{y}_{wj}$ and the bounce slip $\dot{z}_{wj}$ (up and down motion of the wheel) are both unknown quantities and contribute to the unknown vector $\tilde{\dot{\nu}}_w$ in Eq. (8a). The wheel orientation rate quantities consist of $(\dot{\alpha}_{wj}, \dot{\beta}_{wj}, \dot{\gamma}_{wj})$, which are, respectively, tilt slip, sway slip, and turn slip. Due to mechanical constraints, $\dot{\alpha}_{wj} = \dot{\beta}_{wj} = 0$ are known, and the turn slip is an unknown quantity. Consequently, the unknown and known wheel velocity vectors in Eq. (8a) are $\tilde{\dot{\nu}}_{wj} = (r\dot{\vartheta}_{wj} \;\; \dot{y}_{wj} \;\; \dot{z}_{wj} \;\; \dot{\gamma}_{wj})^T$; $\tilde{\dot{\nu}}_w = (\tilde{\dot{\nu}}_{w1} \;\; \tilde{\dot{\nu}}_{w2} \;\; \tilde{\dot{\nu}}_{w3} \;\; \tilde{\dot{\nu}}_{w4})^T$; $\bar{\dot{\nu}}_{wj} = (\dot{\alpha}_{wj} \;\; \dot{\beta}_{wj})^T$; and $\bar{\dot{\nu}}_w = (\bar{\dot{\nu}}_{w1} \;\; \bar{\dot{\nu}}_{w2} \;\; \bar{\dot{\nu}}_{w3} \;\; \bar{\dot{\nu}}_{w4})^T$. The actuated quantities to be determined, that is, $\tilde{\dot{\eta}}$ in Eq. (8a), are the hip angle rates $\dot{\sigma}_1$ and $\dot{\sigma}_2$ and steering angular rates of the four steerable wheels $\dot{\psi}_j, j = 1, 2, 3, 4$. The compliant joint is the differential angle rate $\dot{\rho}$. Thus, $\tilde{\dot{\eta}} = (\dot{\sigma}_1 \;\; \dot{\sigma}_2 \;\; \dot{\psi}_1 \;\; \dot{\psi}_2 \;\; \dot{\psi}_3 \;\; \dot{\psi}_4)^T$ is the unknown actuation vector, and $\bar{\dot{\eta}} = \dot{\rho}$ is

https://doi.org/10.1017/S0263574718001431 Published online by Cambridge University Press

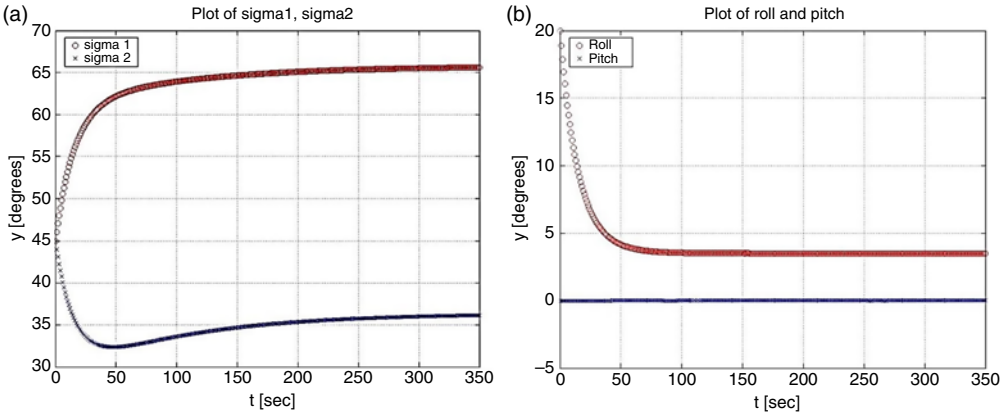

Fig. 8. Trajectories of rover hip angles (a) and body roll and pitch (b) for an inclined terrain.

the known/measured quantity. The excess of unknown over known number of variables is used for the optimization of Eqs (9) and (10).

4.4. Simulation results

In this section we investigate the behavior and performance of the SRR moving on different terrains. In each case, the trajectories of the rover heap joint angles σ_1 and σ_2, body roll α_b, pitch β_b, and the tracking errors are provided. The tracking longitudinal and lateral errors are the differences between the desired rover path specified in (x, y) plane and the actual path traversed by the rover. The elevation z is dictated by the terrain. It must be emphasized that the actuation kinematics discussed in the previous sections determines the set points (reference values) for the hip joints, wheel sheerings, and wheel speed controllers. However, we did not include a direct local feedback control scheme, and thus the results to be given in the following sections are for the actuation kinematics as we only discuss kinematic simulation and animation in this paper. The strategies for the control of articulated rovers, for example, adaptive, predictive, etc., and their dynamic stability are distinct issues and not part of this study. Despite this, the tracking errors are reasonable, as we will see.

4.4.1. Inclined terrain. In this case, the rover traverses along a straight line on an inclined flat surface with a downhill slope of 45° as shown in Fig. 4a, and the rover moves across the terrain where one side of the rover is on higher elevation than the other side. The optimization function parameters in Eq. (9) are chosen as $a_1 = 0.6$, $a_2 = 6$, and $a_3 = 0.6$, respectively. The coefficient of the rover roll a_2 in this case is higher than the other two coefficients to place more emphasis on the roll.

Initially the half hip angles are at their nominal values of $\sigma_1 = \sigma_2 = 45°$. Note that the full hip angles are $2\sigma_1$ and $2\sigma_2$, as explained before. The heap angle trajectories are shown in Fig. 8a and indicate that because one side of the rover is on a higher elevation, its hip angle is increased to 66°, while the hip angle of the other side decreased to about 36° to maintain the rover body level. The trajectories of the body roll α_b and pitch β_b are shown in Fig. 8b and indicate that the roll is quickly reduced from the initial 20° to about 3.5°, while the pitch remains at 0 since the rover moves across the slope and not up or down the slope. These make the body to level. The error between the desired path and the actual path traversed by the rover in this case is very small both in x and y directions with a maximum error of about 3 cm on a 10-m-long path, which is about a tenth of the rover width, despite having no local feedback control. This is due to the simple straight line path on a flat surface. When the terrain has bumps, the errors can be larger, as we will see in the next cases.

4.4.2. Wavy and bumpy terrain. The terrain to be considered for this case is shown in Fig. 4c, where one side of the rover moves over a sinusoidal shape terrain and the other side traverses a smooth bump. The balancing parameters are set to $a_1 = 0.1$, $a_2 = 2$, and $a_3 = 0.1$.

The half hip joint angles are initially at their nominal values of $\sigma_1 = \sigma_2 = 45°$. As the rover wheels on the left side move on ditches and bumps, the hip angles vary to keep the rover as flat as possible

https://doi.org/10.1017/S0263574718001431 Published online by Cambridge University Press

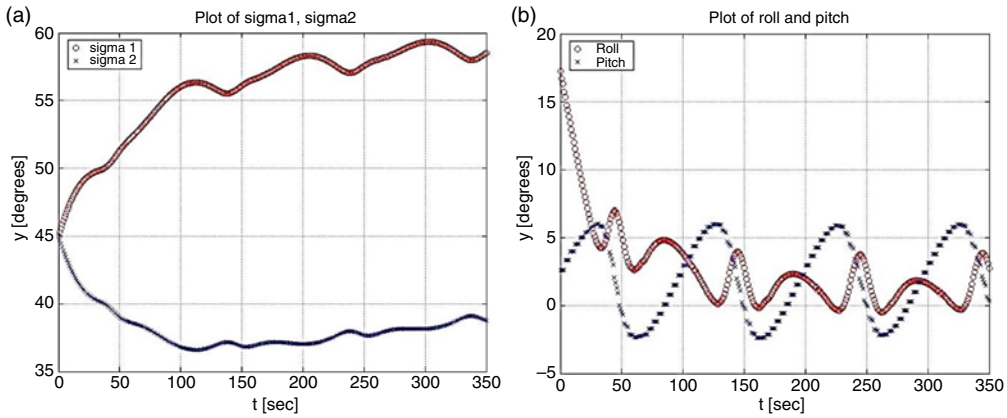

Fig. 9. Trajectories of hip angles (a) and roll and pitch (b) for a wavy and bumpy terrain.

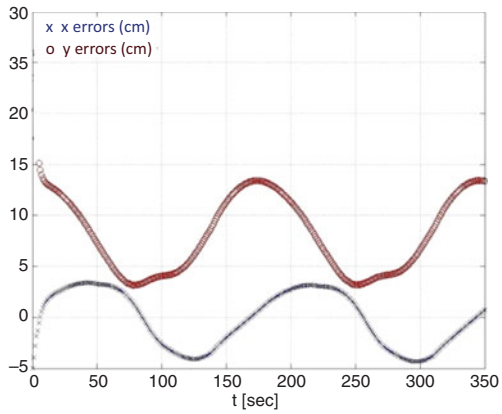

Fig. 10. Error trajectories in x and y directions for a wavy and bumpy terrain.

and avoid tip-over, as seen in Fig. 9a. The variations of the hip angle on the left side σ_1 are much higher than those on the right side σ_2 due to the bumps and ditches, though some of the sinusoidal-like motions also spill to the right side due to the differential mechanism. The pitch and roll are shown in Fig. 9b. The initial value of the body roll α_b is about 18°, and due to balancing it is reduced and its variations will remain in the range of about 4.5°. The body pitch is small and varies about 8°. All these values are well within the stability limits.

The trajectories of tracking errors in the x (longitudinal error) and y directions (lateral error) are shown in Fig. 10. The maximum error in x direction is about 15 cm and in y direction is about 5 cm with the maximum total error, that is, distance of the rover from the desired path at any time during the traversal, of about 17 cm. This error is relatively small considering that the width of the SSR is 40 cm, the leg length is 30 cm, and the traveled path is about 10 m.

4.4.3. Natural rough terrain. This case study demonstrates the performance of the rover traversing a natural terrain that is shown in Fig. 4f, with the balancing parameters in Eq. (9) as $a_1 = 0.3$, $a_2 = 5$, and $a_3 = 1$. As in previous cases, the half hip angles are initially set at their nominal values of $\sigma_1 = \sigma_2 = 45°$. Around the time $t = 35$ s from the start, the left side is on a bump as seen in the close-up view of Fig. 11a, and its hip angle σ_1 extends (increases) to lower the left side and its right hip contracts (decreases) to raise the right side as recorded in Fig. 12a to prevent tip-over. The roll variations are small, but due to the rough terrain the pitch increases up to 27° despite the actions of the hip joints. Even though these variations are within safe limits, the results indicate that with only two hip angles, keeping the rover balanced becomes a challenge in rough terrains. This experiment demonstrates the usefulness of the proposed modeling and simulation and indicates that for rough terrains, such as those shown in the close-up side view of Fig. 11a and the rear view of Fig. 11b, a more sophisticated suspension system such as rocker-bogie would be required.

https://doi.org/10.1017/S0263574718001431 Published online by Cambridge University Press

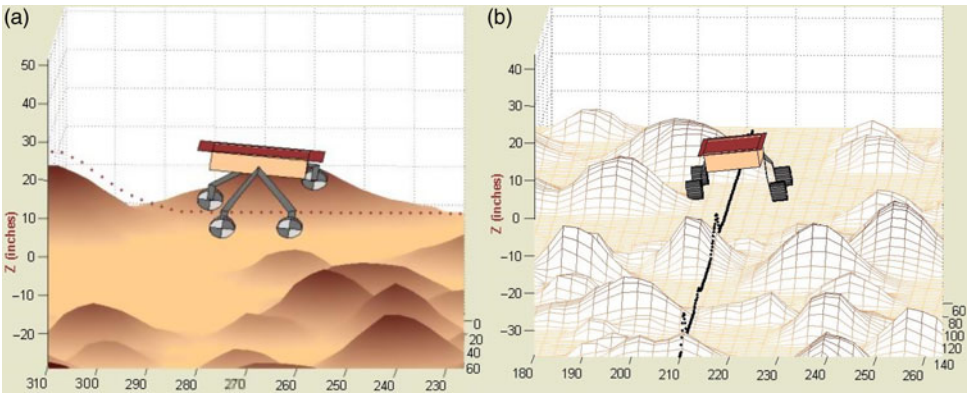

Fig. 11. Two close-up views of the rover moving on a natural rough terrain: (a) side view and (b) rear view.

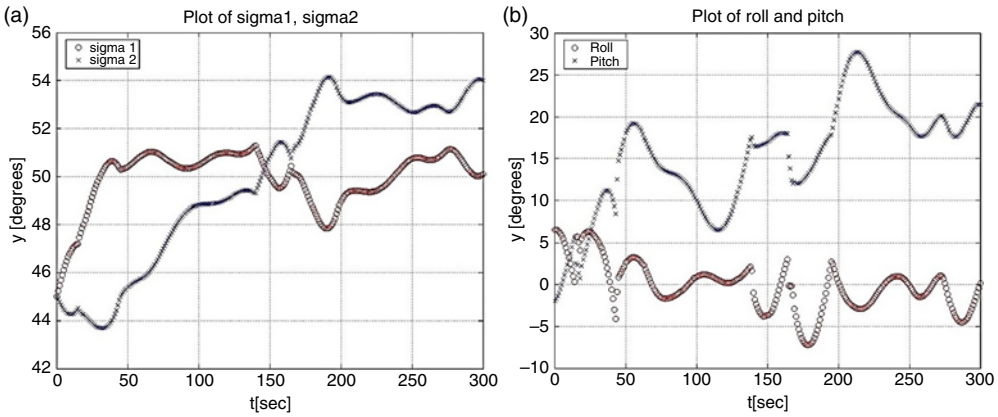

Fig. 12. Trajectories of hip angles (a) and roll and pitch (b) for a rough natural terrain.

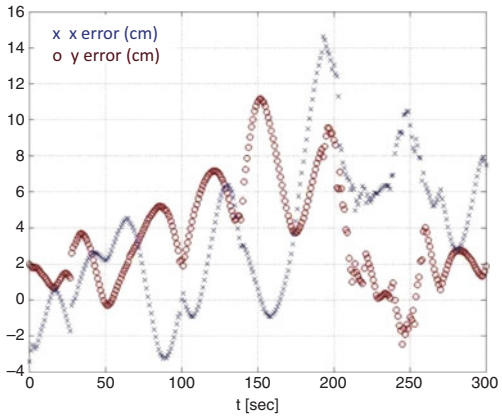

Fig. 13. Error trajectories in x and y directions for a natural rough terrain.

The trajectories of tracking errors in x and y directions are shown in Fig. 13. The maximum error in x is about 15 cm and in y is about 11 cm with the maximum total error, that is, distance from the desired path at any time during the traversal, of about 20 cm, which is half the width of the rover. Considering again that the traveled path is about 10 m long, and the terrain is quite bumpy, the distance error is not high. However, we must also note that there is no guarantee that for longer traversals the errors will be bounded within these limits, since the actuation provides only the set point (reference values) for the motor controllers without direct feedback control.

https://doi.org/10.1017/S0263574718001431 Published online by Cambridge University Press

5. Conclusions

We investigated kinematic modeling of highly articulated rovers that are versatile to operate in natural rough terrains such as those used in space, agriculture, and search-and-rescue operations. These rovers have complex mechanisms to enable them to traverse over rough terrains, and this in turn makes their analysis and synthesis complicated and challenging. By developing the mobility model and a comprehensive simulation and animation environment, the proposed development makes it possible to investigate the performance of rovers in environments with different topologies. The modeling, simulation, and animation developed in this paper were applied to a space exploration rover. The results demonstrate the correctness of the analysis and the usefulness of the approach.

The theoretical kinematic developments and their implementations reported in this paper are quite general and can be applied to any rover. This work not only enables investigating an existing rover and its performance, it also makes it possible to change the suspension mechanism parameters easily and observe the results quickly. This is useful for the design of a new rover or for redesigning an existing rover for improved performance.

The proposed method can be enhanced by incorporating a model of wheel–terrain interaction using terra-mechanics. In addition, for modeling future rovers with fast motions, the dynamics of the rover could be included.

References

1. K. Iagnemma, S. Kang, H. Shibly and S. Dubowsky, "On-line terrain parameter estimation for planetary rovers," *IEEE Trans. Rob.* **20**(2), 921–927 (2004).
2. G. Ishigami, A. Miwa, K. Nagatani and K. Yoshida, "Terramechanics-based model for steering maneuver of planetary exploration rovers on loose soil," *J. Field Rob.* **24**(3), 233–250 (2007).
3. R. Gonzales and K. Iagnemma, "Slippage estimation and compensation for planetary exploration rovers. State of the art and future challenges," *J. Field Rob.* **35**(4), 564–577 (2018).
4. T. Xiaoer and J. Hehua, "Modeling and Simulation for Lunar Rover Based on Terramechanics and Multibody," *Proceedings of the 32nd Chinese Control Conference*, Xi'an, China (2013) pp. 8687–8692.
5. A. Azimi, J. Kovecses and J. Angeles, "Wheel–soil interaction model for rover simulation and analysis using elastoplasticity theory," *IEEE Trans. Rob.* **29**(5), 1271–1288 (2013).
6. H. Gao, W. Li, L. Ding, Z. Deng, Z. Liu and J. Guo, "Algorithm Analysis for a Rover Simulation Platform," *International Conference on Electronic and Mechanical Engineering and Information Technology*, Harbin, China (2011) pp. 666–669.
7. Y.-C. Yang, J.-S. Baol, Y. Jin and Y.-L. Cheng, "A virtual simulation environment for lunar rover: Framework and key technologies," *Int. J. Adv. Rob. Syst.* **5**(2), 201–208 (2008).
8. F. Zhou, R. E. Arvidson, K. Bennett, R. Lindemann, P. Belluta, K. Iagnema and C. Senatore, "Simulations of Mars rover traverses," *J. Filed Rob.* 31(1), 141–160 (2014).
9. T. Flessa, E. McGookin and D. Thomson, "Numerical Stability of Inverse Simulation Algorithms Applied to Planetary Rover Navigation," *Proceedings of the 24th Mediterranean Conference on Control and Automation*, Athens, Greece (2016) pp. 901–906.
10. K. Worrall, D. G. Thomson, E. W. McGookin and T. Flessa, "Autonomous Planetary Rover Control using Inverse Simulation," *13th Symposium on Advanced Space Technologies in Robotics and Automation*, Noordwijk, Netherlands (2015) pp. 724–729.
11. T. Oikawa1, J. Walker and K. Yoshida, "Experimental Evaluation of Thermal Simulation Model for Lunar Exploration Rover," *Proceedings of IEEE/SICE International Symposium on System Integration*, Nagoya, Japan (2015) pp. 882–887.
12. J. F. Archila, M. Moreira, V. I. Van Halts, L. A. Neto Alves, O. E. Rueda and M. Becker, "Simulation of Rovers for Precision Agriculture," *Proceeding of Joint Conference on Robotics: SBR-LARS Robotics Symposium and Robocontrol*, Sao Carlos, Brazil (2014) pp. 229–234.
13. P. T. Schenker, T. L. Huntsberger, P. Pirjanian, E. Baumgartner and E. Tunstel, "Planetary rover developments supporting Mars exploration, sample return and future human robotic, colonization," *J. Auton. Rob.* **14**, 103–126 (2003).
14. R. Volpe, "Rover Functional Autonomy Development for Mars Mobile Science Vehicles," *Proceeding of IEEE Aerospace Conference*, Big Sky, MT, USA (2003) pp. 643–652.
15. A. J. Baerveldt (ed.), "Agricultural Robotics," **In:** *Autonomous Robots*, vol. 13-1 (Kluwer Academic Publishers, Dordrecht, Netherlands, 2002).
16. K. Iagnemma and S. Dubowski, "Traction control of wheel mobile robots in rough terrain with applications to planetary rovers," *Int. J. Rob. Res.* 23(10-11), 1029–1040 (2003).
17. M. Tarokh, G. McDermott, S. Hayati and J. Hung, "Kinematic Modeling of a High Mobility Mars Rover," *Proceedings of the IEEE International Conference on Robotics and Automation*, Detroit, MI, USA (1999) pp. 992–998.
18. M. Tarokh and G. McDermott, "Kinematics modeling and analysis of articulated rovers," *IEEE Trans. Rob.* **21**(4), 539–553 (2005).

https://doi.org/10.1017/S0263574718001431 Published online by Cambridge University Press

19. G. McDermott, M. Tarokh and L. Mireles, "Balance control of articulated rovers with active suspension systems," *Proceedings of the 7th IFAC International Conference on Robot Control*, Bologna, Italy (2006) vol. 8, Pt. 1.
20. M. Tarokh, H. D. Ho and A. Bouloubasis, "Systematic kinematics analysis and balance control of high mobility rovers over rough terrain," *Rob. Auton. Syst.* **61**(1), 13–24 (2013).
21. J. Craig, *Introduction to Robotics – Mechanics and Control* (Pearson Publishers, London, England, 2018) pp. 72–75.
22. N. Nakamura, *Advanced Robotics-Redundancy and Optimization*, Chapter 4 (Addison-Wesley, Boston, 1991).

https://doi.org/10.1017/S0263574718001431 Published online by Cambridge University Press